

## Quantitative structure–retention relationship analysis of nanoparticle compounds

H. Noorizadeh\* and A. Farmany

<sup>1</sup>- Department of Chemistry, Ilam Branch, Islamic Azad University, Ilam, Iran

Received May 2011; Accepted July 2011

### ABSTRACT

Genetic algorithm and partial least square (GA-PLS), the kernel PLS (KPLS) and Levenberg-Marquardt artificial neural network (L-M ANN) techniques were used to investigate the correlation between retention time (RT) and descriptors for 15 nanoparticle compounds which obtained by the comprehensive two dimensional gas chromatography system (GC × GC). Application of the dodecanethiol monolayer-protected gold nanoparticle (MPN) column was for a high-speed separation as the second column of GC × GC. The L-M ANN model with the final optimum network architecture of [9-4-1] gave a significantly better performance than the other models. This is the first research on the quantitative structure–retention relationship (QSRR) of the nanoparticle compounds using the GA-PLS, GA-KPLS and L-M ANN.

**Keywords:** Nanoparticle compounds; Retention time; Dodecanethiol; Genetic algorithm

### INTRODUCTION

Nanoscience Nanoparticles have attracted extensive attention in various fields of chemistry, physics and medicine due to their novel and fascinating properties. In separation science, nanoparticles have been shown to be used as novel stationary phases to provide high separation efficiencies for various analytes. Because the nanoparticles are too small to be packed into the column, they were used mostly as pseudostationary phases to enhance separation performance [1-3]. The development of novel stationary phases for gas chromatography (GC) is an ongoing interest due to the broad scope of applicability of GC methods. The recently developed separation technique, comprehensive two-dimensional gas chromatography (GC×GC), is a powerful technique and very suited to the separation of complex mixtures [4-7]. In (GC×GC) often, a non-polar stationary phase is used for the first column, but since the square capillary MPN column is more appropriately configured for the second column, a polar poly (ethylene glycol) column was used for the first column [8].

The nanoparticles we have been studying are known as gold-centered monolayer protected nanoparticles (MPNs) that consist of a gold core with a thiol-linked monolayer of organic molecules on the surface of the gold core [9, 10]. Potential areas of application for MPNs are demonstrated including complementary separations such as GC × GC [11]. The MPN material provided comparable separation efficiencies as a commercial polymeric stationary phase and was satisfactorily robust with a useful lifetime.

Quantitative structure–retention relationship (QSRR) models are mathematical equations relating chemical structure to their property. A number of reports, deals with QSRR retention time calculation of several compounds have been published in the literature [12, 13]. The QSRR models apply to partial least squares (PLS) method often combined with genetic algorithms (GA) for feature selection [14, 15]. Because of the complexity of relationships between the property of molecules and structures, nonlinear models are also used to model the structure–property relationships. Levenberg-Marquardt artificial neural network

\* Corresponding author: Hadinoorizadeh@yahoo.com

(L-M ANN) and as kernel partial least squares (KPLS) are nonparametric nonlinear models technique that has attracted increasing interest. The basic idea of KPLS is first to map each point in an original data space into a feature space via nonlinear mapping and then to develop a linear PLS model in the mapped space. According to Cover's theorem, nonlinear data structure in the original space is most likely to be linear after high-dimensional nonlinear mapping [15]. Therefore, KPLS can efficiently compute latent variables in the feature space by means of integral operators and nonlinear kernel functions. Compared to other nonlinear methods, the main advantage of the kernel based algorithm is that it does not involve nonlinear optimization. It essentially requires only linear algebra, making it as simple as the conventional linear PLS. In addition, because of its ability to use different kernel functions, KPLS can handle a wide range of nonlinearities. The present study is a first research on QSRR of the nanoparticle compounds against the RT, using GA-PLS, GA-KPLS and L-M ANN.

## THEORY

### Data set

Retention time (RT) of 15 nanoparticle compounds were taken from the literature [8] are presented in Table 1. Sample components are separated, identified, and measured by the GC × GC using the dodecanethiol MPN stationary phase. Dodecanethiol MPNs, in which the

monolayer is dodecanethiol linked to the gold nanoparticle, have shown great promise as a GC stationary phase with efficient columns having been produced in a variety of capillary with stationary phase film depths ranging from 10 to 60 nm, ±2 nm at a given film depth. The GC × GC separation was obtained using a 4m poly (ethylene glycol) column (200 μm i.d., 0.2 μm film) as the first column at 34,000 Pa (40 cm/s) with 0.9m of the dodecanethiol MPN 100 μm square capillary column as the second column operated at 210,000 Pa (235 cm/s). In this study, retention data was resulted by polar capillary (dodecanethiol MPN stationary phase) used for QSRR research.

### Descriptor Calculation

All structures were drawn with the HyperChem software (version 6). Optimization of molecular structures was carried out by semi-empirical AM1 method using the Fletcher-Reeves algorithm until the root mean square gradient of 0.01 was obtained. Since the calculated values of the electronic features of molecules will be influenced by related conformation. In the current research an attempt was made to use the most stable conformations. Some electronic descriptors such as polarizability, dipole moment and orbital energies of LUMO and HOMO were calculated by the HyperChem software. Also optimized structures were used to calculate 1497 descriptors by DRAGON software Version 3.

**Table 1.** The data set and the corresponding observed and predicted RT values by L-M ANN

No.	Name	RT <sub>Exp</sub>	RT <sub>Cal</sub>	RE	SE
1	Hexane	0.43	0.42	1.88	0.02
2	2-Pentanone	0.44	0.48	8.70	0.01
3	Benzene	0.45	0.49	8.33	0.01
4	Octane	0.48	0.47	1.79	0.01
5	2-Butanol	0.48	0.52	7.88	0.01
6	Toluene	0.49	0.45	8.84	0.01
7	1,1,2-Trichloroethane	0.55	0.53	2.95	0.01
8	Ethylbenzene	0.58	0.62	6.26	0.00
9	1-Pentanol	0.61	0.55	9.80	0.01
10	Anisole	0.77	0.71	7.22	0.00
11	4-Ethyltoluene	0.81	0.76	5.95	0.01
12	Decane	0.82	0.77	6.02	0.01
13	Mesitylene	0.85	0.87	2.07	0.01
14	1,2,4-Trimethylbenzene	0.99	0.94	4.56	0.02
15	Bromoheptane	1.04	0.98	6.02	0.02

## RESULTS AND DISCUSSION

### Linear model

#### Results of the GA-PLS model

The best model is selected on the basis of the highest multiple correlation coefficient leave-group-out cross validation (LGO-CV), the least root mean squares error (RMSE), standard error (SE), absolute error (AbsE) and relative error (RE) of prediction and simplicity of the model. These parameters are probably the most popular measure of how well a model fits the data. The best GA-PLS model contains 10 selected descriptors in 6 latent variables space. The obtained statistic parameters of the GA-PLS model were shown in details Table 2. Fig.1 Plot of the GA-PLS calculated values of RT against the experimental values.

**Table 2.** The statistical parameters of different constructed QSRR models

Model	R <sup>2</sup>	RE	AbsE	RMSE	SE
GA-PLS	0.872	11.02	0.8	0.10	0.05
GA-KPLS	0.894	10.31	0.8	0.09	0.06
L-M ANN	0.962	5.88	0.4	0.04	0.01

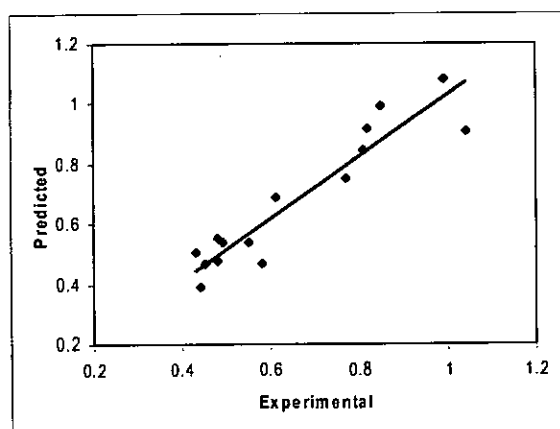


**Fig.1.** Plot of predicted RT obtained by GA-PLS against the experimental values.

### Nonlinear models

#### Results of the GA-KPLS model

In this paper a radial basis kernel function,  $k(x,y) = \exp(-\|x-y\|^2/c)$ , was selected as the kernel function with  $c = rm\sigma^2$  where  $r$  is a constant

that can be determined by considering the process to be predicted (here  $r$  set to be 1),  $m$  is the dimension of the input space and  $\sigma^2$  is the variance of the data [16]. It means that the value of  $c$  depends on the system under the study. The 9 descriptors in 4 latent variables space chosen by GA-KPLS feature selection methods were contained. Table 2 shows the statistical parameters of the results, attained by these models studies for the same set of nanoparticle compounds. Plots of predicted RI versus experimental RI values by L-M ANN are shown in Fig.2. The RMSE values of the GA-KPLS model was much lower than GA-PLS model. This suggests that GA-KPLS hold promise for applications in choosing of variable for L-M ANN systems.

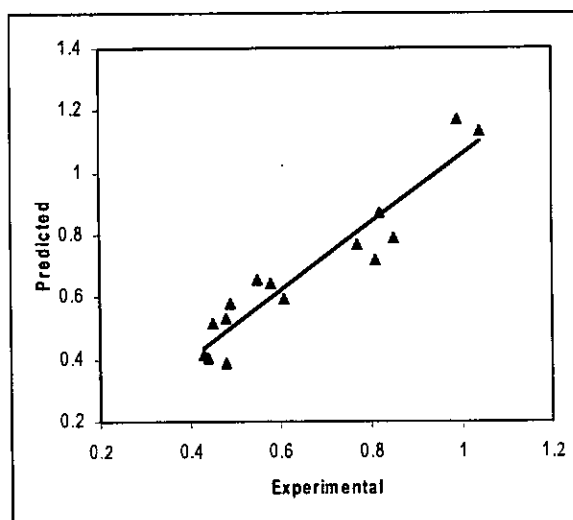


**Fig.2.** Predicted vs. experimental RT by GA-KPLS.

#### Results of the L-M ANN model

With the aim of improving the predictive performance of nonlinear QSRR model, L-M ANN modeling was performed. The network architecture consisted of nine neurons in the input layer corresponding to the nine mentioned descriptors. The output layer had one neuron that predicts the RT. It was realized that the RMSE is minimum when four neurons were selected in the hidden layer. It was realized that after 15 iterations, the RMSE was minimum. The values of experimental, calculated, percent relative error and absolute error are shown in Table 1. Table 2 shows the statistical parameters for the compounds obtained by applying models. The statistical parameters obtained by LGO-CV for

three models are compared in Table 2. Inspection of the results of the table reveals a higher  $R^2$  value and lower RMSE and RE for L-M ANN model compared with their counterparts for GA-KPLS and linear model. Plots of predicted RT versus experimental RT values by L-M ANN are shown in Fig.3. Obviously, there is a close agreement between the experimental and predicted RT and the data represent a very low scattering around a straight line with respective slope and intercept close to one and zero. This clearly shows the strength of L-M ANN as a nonlinear feature selection method.

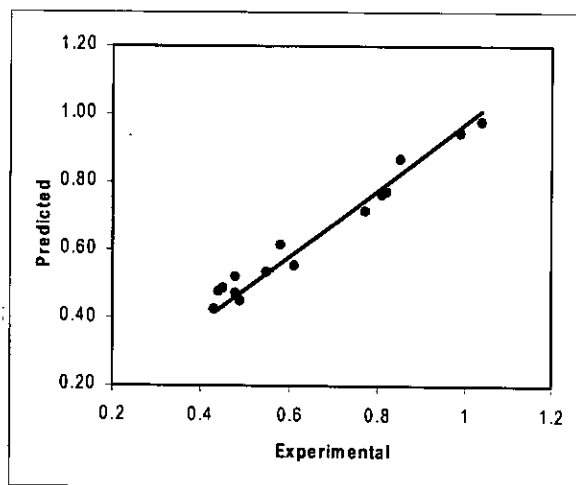


Fig.3. Plot of predicted RT obtained by L-M ANN against the experimental values.

## CONCLUSION

In this research, an accurate QSRR model for estimating the retention time (RT) of nanoparticle compounds was developed by employing the one linear model (GA-PLS) and two nonlinear models (GA-KPLS and L-M ANN). In comparison with models, the results showed that the L-M ANN model can be effectively used to describe the molecular structure characteristic of these compounds. It can also be used successfully to estimate the RT for new compounds or for other compounds whose experimental values are unknown. This indicates that RT of nanoparticles possesses some nonlinear characteristics.

## REFERENCES

- [1] G. Tolnai, G. Alexander, Z. Horvolgyi, Z. Juvancs, A. Dallos, *Chromatographia*. 53 (2001) 69.
- [2] P. Viberg, M. Jornten-Karlsson, P. Petersson, P. Spegel, S. Nilsson, *Anal. Chem.* 74 (2002) 4595.
- [3] K. J. Reynold, L. A. Colon, *J. Chromatogr. Relat. Technol.* 23 (2000) 161.
- [4] F. Adam, F. Bertocini, N. Brodusch, E. Durand, D. Thiebaut, D. Espinat, M.C. Hennion, *J. Chromatogr. A*, 1148 (2007) 55.
- [5] M. Deursen, J. Beens, J. Reijenga, P. Lipman, C. Cramers, J. Blomberg, *J. High Resolut. Chromatogr.* 23 (2000) 507.
- [6] J. Dalluge, J. Beens, U. A. Th. Brinkman, *J. Chromatogr. A*. 1000 (2003) 69.
- [7] G. A. Eiceman, J. Gardea-Torresdey, E. Overton, K. Carney, F. Dorman, *Anal. Chem.* 74 (2002) 2771.
- [8] G. M. Gross, J. W. Grate, R. E. Synovec, *J. Chromatogr. A*. 1029 (2004) 185.
- [9] M. C. Daniel, D. Astruc, *Chem. Rev.* 104 (2004) 293.
- [10] C. Templeton, M. P. Wuelfing, R. W. Murray, *Acc. Chem. Res.* 33 (2000) 27.
- [11] C. Lewis, J.F. Hamilton, C.N. Rhodes, J. Halliday, K.D Bartle, P. Homewood, R. J. P. Grenfell, B. Goody, A.M. Harling, P. Brewer, G.Y. Vargha, M. J. T. Milton, *J. Chromatogr. A*. 1217 (2010) 768.
- [12] J. Chen, T. Yang, S.M. Cramer *J. Chromatogr. A*. 1177 (2008) 207. H. Noorizadeh, A. Farmany, *Chromatographia*, 72 (2010) 563.
- [13] H. Noorizadeh, M. Noorizadeh, *Med Chem Res*, 2011, In press.
- [14] H. Noorizadeh, S. Sobhan Ardakani, T. Ahmadi, S. S. Mortazavic, M. Noorizadchd, *Drug Test Anal*, 2011, In press
- [15] K. Kim, J.M. Lee, I.B. Lee, *Chemom. Intell. Lab. Syst.* 79 (2005) 22.

Photophysical Properties of Electron Transfer Process Between  
1, 3, 5-Trisubstituted Oligoaryleneethynylene Benzene  
Star-Shaped Molecules and Fullerenes

A. Taherpour\*

Department of Chemistry, Arak Branch, Islamic Azad University, Arak, Iran

Received May 2011; Accepted July 2011

ABSTRACT

The star-shaped molecules present some of the important electronic delocalization between the attractive central ring, i.e. benzene, and the three ends  $\pi$ -electron donor groups. The star-shaped molecules are currently considered because of their wide potential applications. Some of them can act as discotic liquid crystals (DLCs). The 1, 3, 5-benzene core acts as an effective  $\pi$ -electron center to conjugate with the oligoaryleneethynylene groups of the 1, 3, 5-trisubstituted oligoaryleneethynylene benzene star-shaped molecules. The electrochemical properties of some of the fullerenes have been studied before. Since the discovery of fullerenes, one of the main classes of carbon compounds, the unusual structures and properties of these molecules and by the many potential applications and physicochemical properties have been discovered and were introduced. In this study, we studied the photophysical properties of the star-shaped molecules 1-9 during the photoelectron transfer (PET) with fullerenes. Some of the photophysical data that were communicated in the literature were: fluorescence emission maximum FEM ( $\lambda_{em}$ ) and absorbance maximum wavelength AMWL ( $\lambda_{abs}$ ). The free energies and the activation free energies and maximum wave length of the PET process, based on the FEM and AMWL amounts,  $\Delta G_{et}$ ,  $\Delta G_{et}^{\#}$  and  $\lambda_{et}$ , respectively, were calculated in this study. The interesting results of the relationships and the photo-physical data of the supramolecular complexes of star-shaped molecules and the selected fullerenes were presented.

**Keywords:** Star-shaped molecule; Fullerenes; Free activation Energies; Hammond's postulate; Marcus theory

INTRODUCTION

The electrochemical properties of the  $C_{60}$  fullerene have been studied since the early 1990s, when these materials first became available in macroscopic quantities. In 1990, Haufler *et al.* [1] showed that  $CH_2Cl_2$  electrochemically reduces  $C_{60}$  to  $C_{60}^{1-}$  and  $C_{60}^{2-}$ . In 1992, Echegoyen *et al.* [2] cathodically reduced  $C_{60}$  in six reversible one-electron steps for -0.97V vs.  $Fc/Fc^+$  ( $Fc$ =ferrocene). This experiment, along with the inability to perform anodic electrochemistry on fullerenes, agrees with the electronic structure of fullerenes: the LUMO of  $C_{60}$  can accept up to six electrons to form  $C_{60}^{6-}$ , but the position of the HOMO does

not allow for hole-doping under the usual reported electrochemical conditions [1, 2].

Star-shaped macromolecules have been investigated as branched macromolecules, and have received significant attention in the elucidation of structure-property relationships [3-12]. Although star polymers constitute a gate group of branched macromolecular structures, the synthesis and study of the properties of star-shaped polymers remains challenging, and well defined star polymers are often difficult to prepare in a controlled manner [7]. Some types of the molecules, with a trivalent core and three poly  $\pi$ -structures, have attracted much attention and been utilized in different areas of science because of their interesting potential, especially

\* Corresponding author: [avatarman.taherpour@gmail.com](mailto:avatarman.taherpour@gmail.com)

for electronic studies. Because of the properties of 1, 3, 5-trisubstituted oligoaryleneethynylene benzene star-shaped molecules, they can act as: *discotic liquid crystals* (DLCs), *light-emitting diodes* (LEDs), *field effect transistors* (FETs), and *non linear optics* (NLO) [3, 4]. Study of the electronic properties of these materials with respect to their photophysical properties can be useful and interesting. Especially with respect to their LED character and quantum yield ( $\Phi_f$ ), only a few reports have been reported in the literature [13-15]. In 2006, the electronic structures and the photophysical properties of 1,3,5-trisubstituted oligoaryleneethynylene benzene star-shaped molecules 1-9 (see Fig.-1) were reported by Y. Yamaguchi et al. [3] In that interesting report, the authors investigated the

photophysical properties, light-emitting characteristics, and occurrence of  $\pi$ -conjugation between the arms of the star-shaped rigid molecules that comprise a 1,3,5-trisubstituted oligoaryleneethynylene benzene star-shaped molecules 1-9 and their methoxy derivatives. Some of the quantities that were reported are: quantum yield ( $\Phi_f$ ), fluorescence emission maximum FEM ( $\lambda_{em}$ ), and absorbance maximum wavelength AMWL ( $\lambda_{abs}$ ) [3, 4, 16, 17].

Graph theory is a sub discipline of mathematics that is closely related to both topology and combinatory concepts. A graph is a topological concept rather than a geometrical concept of fixed geometry, and hence Euclidean metric lengths, angles, and three-dimensional spatial configurations have no importance.

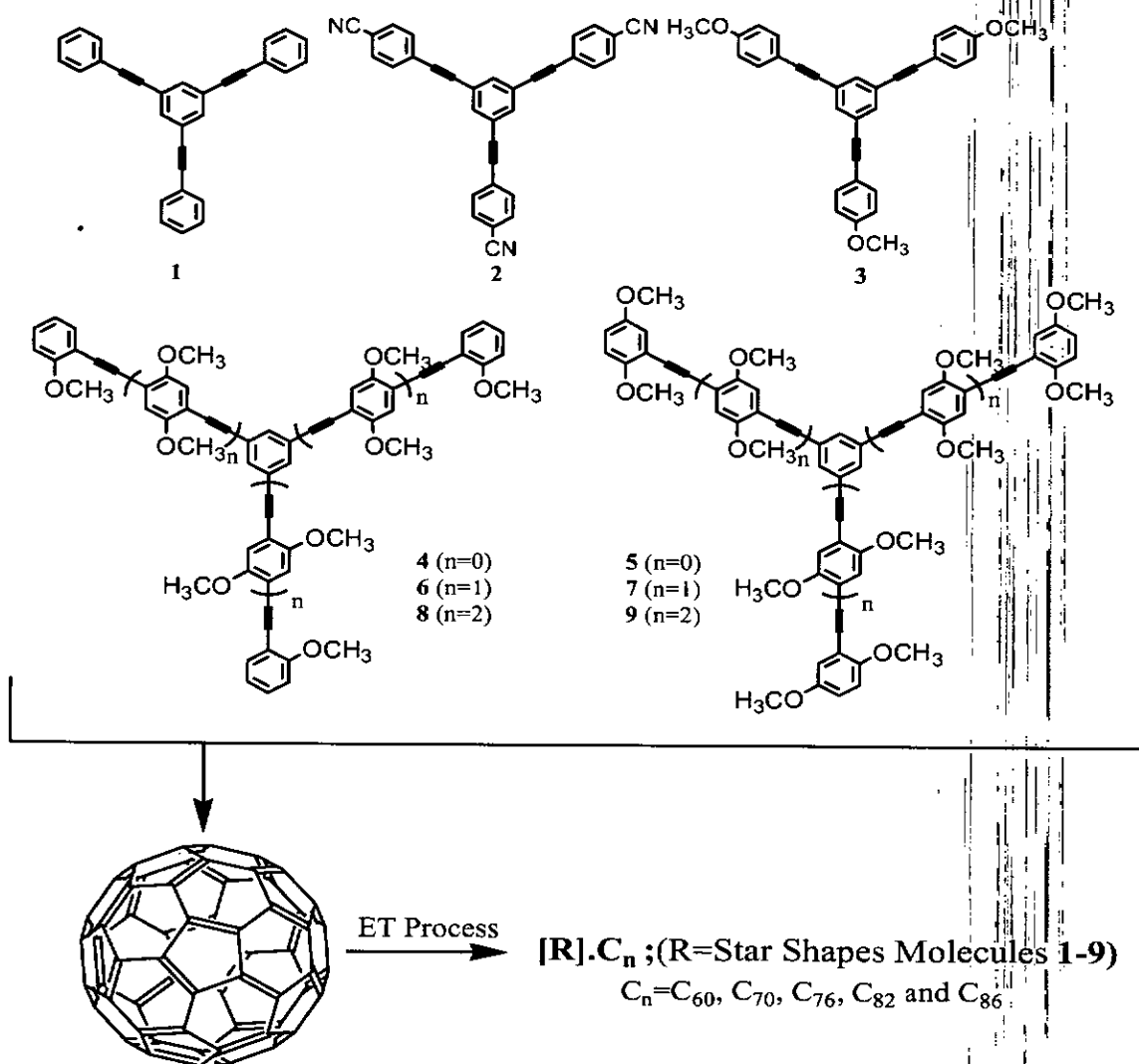


Fig.1. The Structures of 1, 3, 5-trisubstituted oligoaryleneethynylene benzene star-shaped molecules 1-9, the Fullerenes (C<sub>60</sub>, C<sub>70</sub>, C<sub>76</sub>, C<sub>82</sub> and C<sub>86</sub>) and the complexes [R].C<sub>n</sub>.

Aspects of graph theory have been found to be Graph theory is a sub discipline of mathematics that is closely related to both topology and combinatory concepts. A graph is a topological concept rather than a geometrical concept of fixed geometry, and hence Euclidean metric lengths, angles, and three-dimensional spatial configurations have no importance a useful tool in *QSAR* (Quantitative Structure Activity Relationship) and *QSPR* (Quantitative Structure Property Relationship).[4,16,17] The choice of effective, simple structural indices for making good correlations between several data properties is important for the study, extension, and the prediction of properties for these molecules.

Figure-1 shows the Structures of 1, 3, 5-trisubstituted oligoaryleneethynylene benzene star-shaped molecules **1-9**, the Fullerenes ( $C_{60}$ ,  $C_{70}$ ,  $C_{76}$ ,  $C_{82}$  and  $C_{86}$ ) and the complexes [R]. $C_n$ .

In this study, the structural properties of 1,3,5-trisubstituted oligoaryleneethynylene benzene star-shaped molecules **1-9** were used to derive the calculation of the free energies and the activation free energies and maximum wave length of the PET process, based on the fluorescence emission maximum FEM ( $\lambda_{em}$ ), and absorbance maximum wavelength AMWL ( $\lambda_{abs}$ ) amounts,  $\Delta G_{et(n)}$ ,  $\Delta G_{et(n)}^\ddagger$  and  $\lambda_{et}$ , respectively. The interesting results of the relationships and the photo-physical data of the supramolecular complexes of star-shaped molecules and fullerenes [R]. $C_n$  were presented and discussed.

## GRAPHS AND MATHEMATICAL OPERATION

The number of carbon atoms of the star shape molecules was used as a structural index (**1-9**). All graphs and the mathematical operations were performed using *Microsoft Office Excel-2003* programs.

## RESULTS AND DISCUSSION

The electron transfer (ET) equation estimates the free energy change between an electron donor ( $D$ ) and an acceptor ( $A$ ) as

$$\Delta G_{et}^\circ = e[E_D^\circ - E_A^\circ] - \Delta E^* + \omega_1 \quad (\text{Eq.-1})$$

Where "e" is the unit electrical charge,  $E_D^\circ$  and  $E_A^\circ$  are the reduction potentials of the

electron donor and acceptor, respectively,  $\Delta E^*$  is the energy of the singlet or triplet excited state and  $\omega_1$  is the work required to bring the donor and acceptor within the electron transfer (ET) distance. The work term in this expression can be considered to be '0' in so far as an electrostatic complex exists before the electron transfer [18-20].

The Marcus theory of electron transfer implies rather weak (<0.05eV) electronic coupling between the initial (locally excited, LE) and final (electron transfer, ET) states and presumes that the transition state is close to the crossing point of the LE and CT terms. The value of the electron transfer rate constant  $k_{et}$  is controlled by the activation free energy  $\Delta G_{et}^\ddagger$ , which is a function of the reorganization energy ( $I/4$ ) and the electron transfer driving force  $\Delta G_{et}$ :

$$\Delta G_{et}^\ddagger = (I/4) (1 + \Delta G_{et}/I)^2 \quad (\text{Eq.-2})$$

The reorganization energy of organic molecules ranges from 0.1-0.3 eV. In this study, we used the minimum amount of reorganization energy. [18-20]

To calculate the maximum wavelengths ( $\lambda_{(n)}$ ) of the electromagnetic photon for the electron transfer process in the nanostructure supramolecular complexes, we used *Planck's* formula:

$$\Delta G_{et}^\ddagger = \Delta E = h.c/\lambda_{(n)} \quad (\text{Eq.-3})$$

In this study was also used this formula to calculate the activation free energy of the electron transfer process [20].

The information of the photophysical values of 1, 3, 5-trisubstituted oligoaryleneethynylene benzene star-shaped molecules **1-9**, and the number of carbon atoms ( $C_n$ ) were shown in Table-1.

The basic structure of these compounds has the  $C_{30}H_{18}$  formula and is based on the structure **1**. The units with at least  $C_8$  carbon atoms in structures **4-19** were added to each arm of the trivalent benzene cores. The methoxy groups, their position, and the acetylene bonds  $-C\equiv C-$  on the aromatic rings can act as bathochromic groups and oxochromes. The substituted benzene can affect all the photophysical properties of these molecules. With respect to the ortho- and meta- positions of the  $-OMe$  groups, especially in **9**, it seems to be a more

straightforward effect of ortho- and meta-conjugation with benzenes.[3,4] The photophysical data that were reported in the literature were measured in  $\text{CHCl}_3$ . [3,4] By the use of " $\Phi_f$ " some other photophysical data can be calculated [3,4,16,17]. The oxidation potentials of the fullerenes ( $\text{C}_{60}$ ,  $\text{C}_{70}$ ,  $\text{C}_{76}$ ,  $\text{C}_{82}$  and  $\text{C}_{86}$ ) were reported. The  $^{Ox}E_n$  (in Volt) for  $\text{C}_{60}$ ,  $\text{C}_{70}$ ,  $\text{C}_{76}$ ,  $\text{C}_{82}$  and  $\text{C}_{86}$  are: +1.21, +1.19, +0.81, +0.72 and +0.73, respectively. The reduction potentials of the star shape molecules 1-9 were calculated on the basis of the fluorescence emission maximum FEM ( $\lambda_{em}$ ), and absorbance maximum wavelength AMWL ( $\lambda_{abs}$ ) amounts. The values were predicted in Table-1. The

values of the free energies and the activation free energies and maximum wave length of the photoelectron transfer (PET) with the fullerenes, were calculated based on FEM and AMWL amounts,  $\Delta G_{et(n)}$ ,  $\Delta G_{et(n)}^\ddagger$  and  $\lambda_{et}$ , respectively. The calculated values were shown in Table-2. To calculate these values were utilized the equations 1-3. The investigation of the results show that the values of  $\Delta G_{et(n)}$  and  $\Delta G_{et(n)}^\ddagger$  were decreased by increasing the number of carbon atoms and the number of conjugated electron in the structures of star shape molecules and the fullerenes or at the structure of the complexes  $[\text{R}]_n\text{C}_n$ .

**Table 1.** The selected photophysical data (fluorescence emission maximum FEM ( $\lambda_{em}$ ) and absorbance maximum wavelength AMWL ( $\lambda_{abs}$ )) and  $^{Ox}E_{FEM}$  and  $^{Ox}E_{AMWL}$  in Volt of the 1, 3, 5-trisubstituted oligoaryleneethynylene benzene star-shaped molecules 1-9[3, 4]

No.	Molecular Formula	$C_n$	FEM ( $\lambda_{em}$ ) nm*	$^{Ox}E_{FEM}$ in Volt	AMWL ( $\lambda_{abs}$ ) nm*	$^{Ox}E_{AMWL}$ in Volt
1	$\text{C}_{30}\text{H}_{18}$	30	353	-0.296	305	-0.343
2	$\text{C}_{33}\text{H}_{15}\text{N}_3$	33	357	-0.293	320	-0.326
3	$\text{C}_{33}\text{H}_{24}\text{O}_3$	33	360	-0.290	316	-0.331
4	$\text{C}_{33}\text{H}_{24}\text{O}_3$	33	359	-0.291	314	-0.333
5	$\text{C}_{36}\text{H}_{32}\text{O}_6$	36	384	-0.272	334	-0.313
6	$\text{C}_{63}\text{H}_{36}\text{O}_9$	63	406	-0.257	377	-0.277
7	$\text{C}_{69}\text{H}_{64}\text{O}_{12}$	69	409	-0.255	380	-0.275
8	$\text{C}_{93}\text{H}_{80}\text{O}_{15}$	93	433	-0.241	405	-0.258
9	$\text{C}_{96}\text{H}_{104}\text{O}_{18}$	96	464	-0.225	426	-0.245

\*The reported photophysical data were measured in  $\text{CHCl}_3$ . (See Reference [3])

**Table 2.** The values of the activation energies, free activation energies and the maximum wave length of the photoelectron transfer (PET) rate constants ( $\Delta G_{et}$  and  $\Delta G_{et}^\ddagger$  in  $\text{kcal mol}^{-1}$  and  $\lambda_{et}$  in nm) of  $[\text{R}]_n\text{C}_n$ , <sup>a</sup>supramolecular complexes between 1-9 and the selected fullerenes ( $\text{C}_{60}$ ,  $\text{C}_{70}$ ,  $\text{C}_{76}$ ,  $\text{C}_{82}$  and  $\text{C}_{86}$ ). To calculate the values of  $\Delta G_{et}$ ,  $\Delta G_{et}^\ddagger$  and  $\lambda_{et}$  were used the fluorescence emission maximum (FEM)

No	$\text{C}_{60}$			$\text{C}_{70}$			$\text{C}_{76}$			$\text{C}_{82}$			$\text{C}_{86}$		
	$\Delta G_{et}$	$\Delta G_{et}^\ddagger$	$\lambda_{et}$												
1	34.04	50.72	563	33.58	49.65	575	24.81	31.39	909	22.69	27.69	1030	22.97	28.09	1017
2	33.97	50.56	565	33.51	49.47	577	24.74	31.27	913	22.68	27.56	1030	22.89	27.97	1020
3	33.89	50.39	566	33.43	49.32	579	24.30	31.14	917	22.59	27.44	1040	22.82	27.82	1021
4	33.92	50.45	567	33.46	49.38	578	24.69	31.19	916	22.62	27.49	1039	22.85	27.88	1023
5	33.48	49.43	577	33.02	48.37	590	24.24	30.39	940	22.18	26.73	1068	22.41	27.12	1050
6	33.14	48.64	587	32.68	47.58	600	23.91	29.76	960	21.84	26.15	1090	22.06	26.54	1070
7	33.09	48.53	588	32.63	47.48	601	23.86	29.67	962	21.79	26.07	1089	22.02	26.46	1068
8	32.77	47.79	597	32.30	46.75	611	23.54	29.10	981	21.46	25.53	1110	21.69	25.91	1100
9	32.39	46.96	608	31.94	45.92	622	23.18	28.54	1004	21.09	24.92	1150	21.33	25.30	1130

<sup>a</sup> The data for the compounds and their complexes were not reported before.

In Figure 2 was exposed the relationship between  $\Delta G_{et}$  and the number of carbon atoms of the fullerenes in  $[R].C_n$  (R=Star shape molecule (2) and  $n=60, 70, 76, 82$  and  $86$ ) complexes. To this plot the values of  $\Delta G_{et}$  were used the fluorescence emission maximum (FEM). The other graphs for other complexes have similar shapes. The equation 4 demonstrates the relationships between the number "n" of carbon atoms in the fullerenes and the free-energies of electron transfer ( $\Delta G_{et}$ ) of  $[R].C_n$  ( $n = 60, 70, 76, 82$  and  $86$ ). These data were regressed with a third-order polynomial equation. The R-squared value ( $R^2$ ) for the graph is 0.9769.

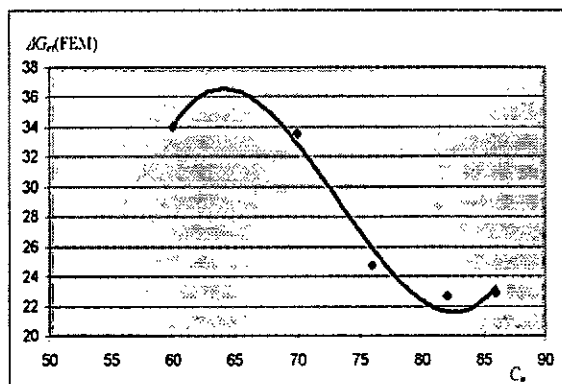


Fig. 2. The relationship between  $\Delta G_{et}$  and the number of carbon atoms of the fullerenes in  $[R].C_n$  (R=Star shape molecule (2) and  $n=60, 70, 76, 82$  and  $86$ ) complexes. To this plot the values of  $\Delta G_{et}$  were used the fluorescence emission maximum (FEM). The other graphs for other complexes have similar shapes.

$$\Delta G_{et} = 0.0047(n)^3 - 1.0395(n)^2 + 75.012(n) - 1745.2 \quad (\text{Eq.-4})$$

The Figure 3 has shown the relationship linking  $\Delta G_{et}^\#$  and the number of carbon atoms of the fullerenes in  $[R].C_n$  (R=Star shape molecule (2) and  $n=60, 70, 76, 82$  and  $86$ ) complexes. In accordance with this scheme the values of  $\Delta G_{et}^\#$  were used the fluorescence emission maximum (FEM). The other related graphs for other complexes have similar structures. The equation 5 has demonstrated the relationships between the number "n" of carbon atoms in the fullerenes and the activation free-energies of electron transfer ( $\Delta G_{et}^\#$ ) of  $[R].C_n$  complexes. These data were regressed with a third-order polynomial equation. The R-squared values ( $R^2$ ) for these graphs are: 0.9732.

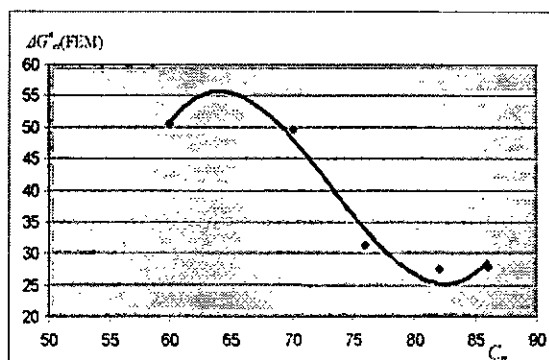


Fig. 3. The relationship between  $\Delta G_{et}^\#$  and the number of carbon atoms of the fullerenes in  $[R].C_n$  (R=Star shape molecule (2) and  $n=60, 70, 76, 82$  and  $86$ ) complexes. To this plot the values of  $\Delta G_{et}$  were used the fluorescence emission maximum (FEM). The other graphs for other complexes have similar shapes.

$$\Delta G_{et}^\# = 0.0097(n)^3 - 2.129(n)^2 + 153.5(n) - 358 \quad (\text{Eq.-5})$$

The relationship between  $\lambda_{et}$  and the number of carbon atoms of the fullerenes in  $[R].C_n$  (R=Star shape molecule (2) and  $n=60, 70, 76, 82$  and  $86$ ) complexes has demonstrated in Figure 4. For the values of  $\lambda_{et}$  was utilized the amounts of the fluorescence emission maximum (FEM). The other related graphs for other complexes have similar forms. The equation 6 has shown the relationships between the number "n" of carbon atoms in the fullerenes and the activation free-energies of electron transfer ( $\Delta G_{et}^\#$ ) of  $[R].C_n$  complexes. These data were also regressed with a third-order polynomial equation. The R-squared values ( $R^2$ ) for these graphs are: 0.9876.

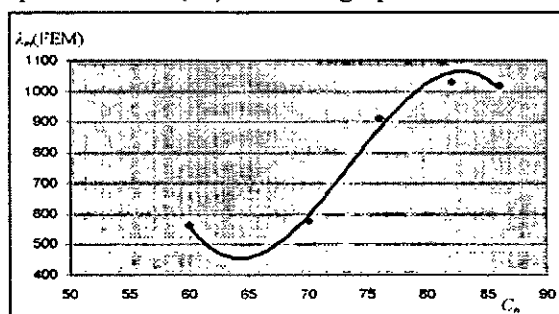


Fig. 4. The relationship between  $\lambda_{et}$  (in nm) and the number of carbon atoms of the fullerenes in  $[R].C_n$  (R=Star shape molecule (2) and  $n=60, 70, 76, 82$  and  $86$ ) complexes. To this plot the values of  $\Delta G_{et}$  were used the fluorescence emission maximum (FEM). The other graphs for other complexes have similar shapes.

$$\lambda_{et} = -0.1885(n)^3 + 41.584(n)^2 - 3009.1(n) + 72115 \quad (\text{Eq.-6})$$

Here was determined the values of the maximum wavelengths ( $\lambda_{(n)}$ ; in nm) for the each stage of the electron transfer process in the nanostructure complexes [R].C<sub>n</sub> with Planck's formula (Eq.-3). Using this formula, we have also determined the activation free energy of the electron transfer process. Most of the values were found in the UV-visible-Near IR (190-800nm and >1200nm) range of the

electromagnetic spectrum. The photophysical data of the complexes [R].C<sub>n</sub> depend on the HOMO-LUMO gap of the 1-9 and the oxidation potentials of the fullerenes have changed. The maximum wavelengths ( $\lambda_{(n)}$ ) depended on the  $\Delta G_{et}^{\#}$  values of the fluorescence emission maximum FEM ( $\lambda_{em}$ ), and absorbance maximum wavelength AMWL ( $\lambda_{obs}$ ) amounts in each stage show regular changes (Equation 3 and Tables 2 & 3).

**Table 3.** The values of the activation energies, free activation energies and the maximum wave length of the photoelectron transfer (PET) rate constants ( $\Delta G_{et}$  and  $\Delta G_{et}^{\#}$  in kcal mol<sup>-1</sup> and  $\lambda_{et}$  in nm) of [R].C<sub>n</sub>,<sup>a</sup> supramolecular complexes between 1-9 and the selected fullerenes (C<sub>60</sub>, C<sub>70</sub>, C<sub>76</sub>, C<sub>82</sub> and C<sub>86</sub>). To calculate the values of  $\Delta G_{et}$ ,  $\Delta G_{et}^{\#}$  and  $\lambda_{et}$  were used the absorbance maximum wavelength (AMWL)

3	C <sub>60</sub>			C <sub>70</sub>			C <sub>76</sub>			C <sub>82</sub>			C <sub>86</sub>		
No.	$\Delta G_{et}$	$\Delta G_{et}^{\#}$	$\lambda_{et}$												
1	35.12	53.30	536	34.70	52.20	547	25.90	33.43	854	23.80	29.60	965	24.05	30.00	952
2	34.72	52.34	545	34.26	51.27	557	25.50	32.69	874	23.43	28.89	988	23.65	29.30	974
3	34.84	52.63	542	34.38	51.53	554	25.61	32.90	868	23.54	29.10	981	23.77	29.51	968
4	34.88	52.74	541	34.42	51.64	553	25.66	32.90	866	23.59	29.18	979	23.82	29.59	965
5	34.42	51.64	553	33.97	50.56	565	25.20	32.13	889	23.13	28.36	1000	23.35	28.77	992
6	32.45	47.06	607	31.98	46.02	620	23.22	28.53	1000	21.15	24.90	1140	21.37	25.37	1130
7	33.55	49.59	576	33.09	48.53	588	24.33	30.51	936	22.25	26.85	1060	22.48	27.25	1050
8	33.16	48.69	586	32.69	47.63	599	23.94	29.80	958	21.86	26.18	1090	22.09	26.58	1070
9	32.86	48.00	595	32.39	46.95	608	23.64	29.27	976	21.56	25.69	1100	21.79	26.07	1090

<sup>a</sup> The data for the compounds and their complexes were not reported before.

Because the rate of chemical reactions are controlled by the free energy of the transition state, information about the structure of transition states (TS) is crucial to understanding reaction mechanism. Because TS has only transitory existence, it is not possible to make experimental measurements that provide direct information about their structure. Hammond's postulate has discussed the circumstances under which it is valid to relate transition state structure [21]. This statement can be discussed with reference to potential energy diagram. See Figures 5 and 6. Figure 5 shows the free energy surfaces of electron transfer  $\Delta G_{et}$  and  $\Delta G_{et}^{\#}$  between 1-9 and the selected fullerenes in the structures of [R].C<sub>n</sub>, which were demonstrated by equations 1-2 and the Hammond's postulate that they were shown in Tables 1-3. Because of the good linear correlations between  $\Delta G_{et}$  and  $\Delta G_{et}^{\#}$  between 1-9 and the selected fullerenes in

the structures of [R] it is possible to extend the results to other similar structures. The free energies of electron transfer and the activation free energies can be calculated with the equations 1 and 2. The R<sup>2</sup> of the linear relationship was very good and equal to 0.9996. The related curves for other complexes [R].C<sub>n</sub> (R=Star shape molecules (2-9) and n=60, 70, 76, 82 and 86) have similar linear structure. See Figure 6. Some of the supramolecular complex structures that were discussed here, the calculated values of the free energies and the activation free energies and maximum wave length of the PET process, based on FEM and AMWL amounts,  $\Delta G_{et}$ ,  $\Delta G_{et}^{\#}$  and  $\lambda_{et}$ , respectively, corresponding to these complexes and the reduction potentials (<sup>Red</sup>E) for the star shape molecules 1-9, were neither synthesized nor reported before.

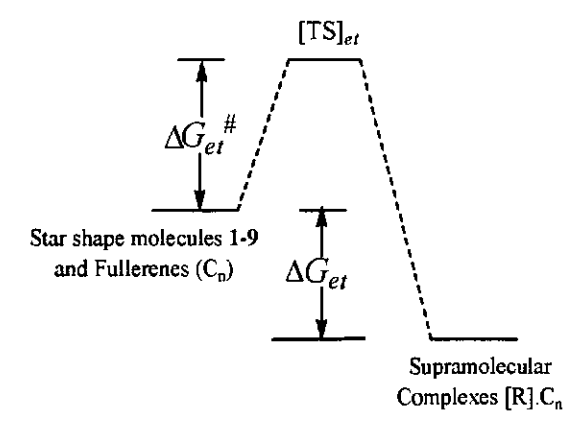


Fig. 5. The surfaces of the free energies of electron transfer  $\Delta G_{et}$  and  $\Delta G_{et}^{\#}$  between the star shape molecules 1-9 and the selected fullerenes in the structures of [R].C<sub>n</sub> complexes.

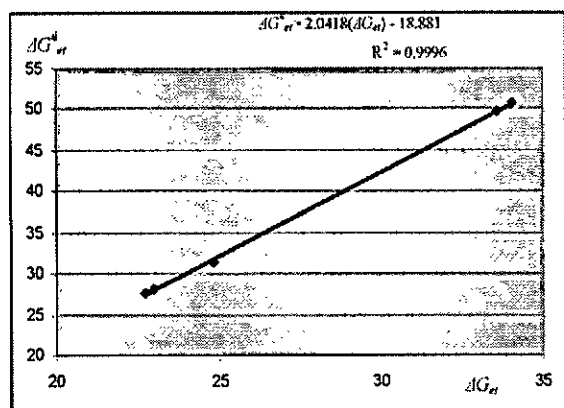


Fig. 6. The linear relationship between  $\Delta G_{et}$  and  $\Delta G_{et}^{\#}$  of [R].C<sub>n</sub> (R=Star shape molecule (1) and n=60, 70, 76, 82 and 86) complexes in accordance with the Hammond's postulate. The related curves for other complexes [R].C<sub>n</sub> (R=Star shape molecules (2-9) and n=60, 70, 76, 82 and 86) have similar linear structure. To this plot the values of  $\Delta G_{et}$  and  $\Delta G_{et}^{\#}$  were used the fluorescence emission maximum (FEM).

## CONCLUSION

The star-shaped molecules demonstrate the important electronic delocalization between the attractive central ring, i.e. benzene, and the three ends  $\pi$ -electron donor groups. The 1, 3, 5 benzene core acts as an effective  $\pi$ -electron center to conjugate with the oligoaryleneethynylene groups of the 1, 3, 5-trisubstituted oligoaryleneethynylene benzene star-shaped molecules (1-9). This work attempted to derive the electrochemical behavior and the photoelectron transfer between 1-9 and

the selected fullerenes. Some of the other values such as the free energies of electron transfer  $\Delta G_{et(n)}$ ,  $\Delta G_{et(n)}^{\#}$  and  $\lambda_{et}$  in the supramolecular complexes [R].C<sub>n</sub> were reported here. The fluorescence emission maximum ( $\lambda_{em}$ ), and the absorbance maximum wavelength ( $\lambda_{abs}$ ) of 1-9 were the basic amounts to calculate the  $\Delta G_{et(n)}$  and  $\lambda_{et}$  in the predicted complexes. By the use of the model and the related equations, it is possible to calculate some of the photophysical data for these complexes in a simple manner and with good approximation.

## ACKNOWLEDGMENT

The author gratefully acknowledges the colleagues in the Research Council of Islamic Azad University of Arak.

## REFERENCES

- [1] RE. Haufler, J. Conceicao, L. P. F. Chibante, Y. Chai, N. E. Byrne, S. Flanagan, et al., *J. Phys. Chem.*, 94 (1990) 8634.
- [2] Q. Xie, E. Perez-Codero, L. Echegoyen, *J. Am. Chem. Soc.*, 114 (1992) 3978.
- [3] Y. Yamaguchi, T. Ochi, S. Miyamura, T. Tanaka, S. Kobayashi, T. Wakamiya, Y. Matsubara and Z.-i. Yoshida, *J. Am. Chem. Soc.*, 128 (2006) 4504. (and the literature cited therein).
- [4] A. Taherpour, *Physics and Chemistry of Liquids*, 48(3) (2010) 289.
- [5] L. E. Casey, V. Kalpana, and E. L. Timothy, *Macromolecules*, 39 (2006) 3132.
- [6] N. Hadjichristidis, *J. Polym. Sci., Part A: Polym. Chem.*, 37 (1999) 857.
- [7] M. R. Tant, G. L. Wilkes, R. F. Storey, J. P. Kennedy, *Polym. Bull. (Berlin)*, 13 (1985) 541.
- [8] P. M. Wood-Adams, J. M. Dealy, A. W. deGroot, G. D. Redwine, *Macromolecules*, 33 (2000) 7489.
- [9] M. G. McKee, S. Unal, G. L. Wilkes, T. E. Long, *Prog. Polym. Sci.*, 30 (2005) 507.

- [10] T. Pakula, P. Minkin, K. Matyjaszewski, *ACS Symp. Ser.*, 854 (2003) 366.
- [11] K. Hatada, T. Kitayama, K. Ute, T. Nishiura, *J. Polym. Sci., Part A: Polym. Chem.*, 42 (2004) 416.
- [12] J. J. Freire, *Adv. Polym. Sci.*, 143 (1999) 35.
- [13] L. Kanibolotsky, R. Berridge, P. J. Skabara, I. F. Perepichka, D. D. C. Bradley and M. Koeberg, *J. Am. Chem. Soc.*, 126 (2004) 13695.
- [14] J. G. Rodriguez, J. Esquivias, A. Lafuente and C. Diaz, *J. Org. Chem.*, 68 (2003) 8120.
- [15] K. Pieterse, A. Lauritson, A. P. H. J. Schenning, J. A. J. M. Vekemans and E. W. Meijer, *Chem.-Eur. J.*, 9 (2003) 5597.
- [16] J. A. Barltrop, J. D. Coyle, "Principles of Photochemistry"; Wiley Publisher, New York, 1978.
- [17] N. Leventis, A.-M. M. Rawashdeh, I. A. Elder, J. Yang, A. Dass, C. Stiriou-Leventis, *Chem. Mater.*, 16 (2004) 1493.
- [18] M. D. Newton, *Chem. Rev.*, 91 (1991) 767.
- [19] R. A. Marcus, N. Sutin, *Biochim. Biophys. Acta.*, 811 (1985) 265.
- [20] P. W. Atkins, "Physical Chemistry", 6th Ed., Oxford University Press, Oxford 1998.
- [21] G. S. Hammond, *J. Am. Chem. Soc.*, 77 (1955) 334. b) F. A. Carey and R. J. Sundberg, "Advanced Organic Chemistry", 4th Ed., Kluwer Academic/Plenum Publishers, New York, USA, P.217.